Synthesis of wall pressure fields of non-homogeneous turbulent boundary layers for vibroacoustic simulations

Corentin Guillon, Emmanuel Redon, Laurent Maxit

Synthesis of wall pressure fields of non-homogeneous turbulent boundary layers for vibroacoustic simulations

Corentin Guillon[a], Laurent Maxit[a], Emmanuel Redon[a,b]

Accepté dans le Journ. of the Acoust. Soc. of America le 15 février 2022
version révisée, peut différer de la version publiée

[a] Univ Lyon, INSA Lyon, LVA, 25 bis av. Jean Capelle, F-69621, Villeurbanne Cedex, France
[b] Université de Bourgogne, ESIREM, 9 av. Alain Savary, BP 47870, F-21078 Dijon, France

Abstract In this paper, a numerical process is presented for predicting the response of vibrating structures excited by a non-homogeneous turbulent boundary layer. This one is based on the synthesis of different realizations of the random pressure fluctuations that can be introduced as loading of a vibroacoustic model. The vibratory response is finally deduced by averaging together the responses of the different loads. As a first approach, the pressure fluctuations of the non-homogeneous turbulent boundary layer can be generated separately for different sub-areas of the structure by using the uncorrelated wall plane waves technique and mean boundary layer parameters. An extension of this basic approach consists in taking into account the interaction between the sub-areas and a refinement of the sub-area decomposition. Wall pressure fluctuations related to a continuous evolution of the boundary layer can then be generated and introduced in the vibroacoustic model. The accuracy of the proposed approach is studied on a rectangular panel excited on one side by a growing fully turbulent boundary layer triggered at one edge of the plate. Comparisons with the spatial approach and the wavenumber approach using the sub-area decomposition technique are proposed. Interests of the proposed approach in term of accuracy and computing times are discussed.

1. Introduction

Vibrations induced by the wall pressure under a turbulent boundary layer is a major concern in the design of vehicles. Such vibrations cause structure wear and are a source of disturbing interior noise. Predicting the vibroacoustic behavior of structures excited by a turbulent flow is an important issue for improving vehicle longevity and passenger comfort.

Most of the literature focusing on the vibratory response of structures excited by turbulent boundary layer (TBL) consider a spatially homogeneous excitation (see for instance Graham (1997); Hambric et al. (2004); De Rosa and Franco (2008); Ciappi et al. (2009); Franco et al. (2013); Maxit and Denis (2013); Ciappi et al. (2016); Marchetto et al. (2018)). However, many industrial applications show vibrating structures underneath a growing TBL or with curved surfaces for which the pressure loading can no longer be considered homogeneous spatially. This situation occurs on the sonar bow of a vessel or on the appendices of a submarine vehicle (steering rods, sail, rudder), on

laurent.maxit@insa-lyon.fr

the windshield and the roof of a passenger car, or on the cockpit of an aircraft to cite few examples. For these cases, the spatial variations of the TBL is generally due to the growing of the TBL from its starting point and to the pressure gradients induced by the curvature of the flow. Few attention has been carried out to this topic whereas the influence of an inhomogeneous TBL can not be negligible on the vibroacoustic behavior of the structure. This has been have recently highlighted by the present authors on a rectangular plate with varying thickness and excited by a TBL triggered at the upstream edge of the plate (Guillon et al., 2021). In this context, this article aims to propose a efficient and versatile process for predicting the vibratory response of a structure excited by a non-homogeneous TBL. This process relies on an extension of the uncorrelated wall plane waves method developed some year ago for homogeneous TBL (Maxit, 2016). It consists in the synthesis of different realizations of the TBL wall pressure field taking into account the spatial variations of the TBL parameters. These realizations can then be easily used as loadings of any vibroacoustic model. For sake of conciseness and simplicity, a flat plate excited by a TBL triggered at one of its edge will be considered as an example. No static pressure gradient will then be considered. That will allow us using models of the wall pressure fluctuation (WPF) developed during these last seventy years as discussed below. Considering a case with pressure gradients would have required the use of dedicated models of the WPF that are currently under developments by teams specialized in fluid mechanics (see for instance Rozenberg et al. (2012); Salze et al. (2014)). As these models are not yet fully validated, it had appeared more relevant for these first developments concerning a structure excited by non-homogeneous TBL excitations to consider a case without pressure gradient.

The phenomena occurring underneath the TBL are random and it generally requires impractical computing time to get the solutions of the Navier-Stokes equations. Direct numerical simulations (DNS) and large eddy simulations (LES) are limited to low Reynolds numbers and canonical flow conditions (Cohen and Gloerfelt, 2018) and are nonviable in terms of time consumption for engineering applications. Many researchers have then focused on the characterization of the power spectral density of the random turbulent pressure, generally from experimental measurements. Wall pressure fluctuation (WPF) models have been established from analytical expressions depending on the TBL parameters and on unknown parameters determined by fitting the model to experimental data for flat surfaces and fully developed TBL with zero pressure gradient (Goody, 2004; Corcos, 1964; Mellen, 1990; Chase, 1980). These models are composed of the auto-spectrum which characterizes the power of the excitation and of the normalized cross-spectrum which expresses the spatial correlation of the pressure fluctuations. Auto-spectrum semi-empirical models are generally built following scaling laws (Ciappi and Magionesi, 2005; Hwang et al., 2009). The space-frequency cross-spectrum, in the case of a spatially homogeneous TBL, is a function of 2-point spatial separation, representing the decay of the correlation (Corcos, 1964; Mellen, 1990). Considering a space Fourier transform of the cross-spectrum, expressions in the wavenumber domain can be obtained like for the Chase model (Chase, 1980).

These models of WPF are generally used for estimating the vibroacoustic response of a panel excited by a TBL. The calculation process can be decomposed in 3 steps:

- a hydrodynamic calculation is used to estimate the TBL parameters as functions of space, from the problem geometry and flow characteristics;
- the WPF spectrum is evaluated with an appropriate model proposed in the literature as described previously and from the space-average of the TBL parameters as an input;
- the vibratory response of the panel is calculated using a vibroacoustic model considering the WPF spectrum as an input.

The main difficulty related to this process is the coupling of the random model of the wall pressure fluctuations induced by the TBL to the deterministic vibroacoustic model. Five methods are discussed in Maxit et al. (2015). Three of them will be used and adapted in this paper to take into account the spatial inhomogeneity of the TBL:

- the first one, the most common, is based on a formulation in the spatial domain. It requires to discretize the panel surface with a fine grid and to estimate the frequency response functions (FRF) between the different points of the grids (Hong and Shin, 2010). As the grid should be sufficiently fine to capture the small variations due to the convection of the vortexes, the number of FRF to be calculate can be high and the computing time can be huge (Ciappi et al., 2012). Alternative methods in discrete coordinates have been proposed to circumvent this issue. For instance, the frequency modulated pseudo-equivalent deterministic excitation ($PEDE_M$) (De Rosa et al., 2015, 2013) can be cited as an effective method for the mid to high frequency ranges. Its fundaments are based on the pseudo excitation method (Xu et al., 1999; Lin et al., 2011), an exact method relying on the modal decomposition of the cross-spectrum at each frequency, and on the introduction of approximations on the WPF spectrum representation in order to reduce significantly the computational costs;

- the second one is based on a wavenumber formulation (Maury et al., 2002). The panel response is estimated through the sensitivity functions that correspond to the panel response to wall plane waves. This method is substantially faster when the convective ridge of the TBL can be neglected, since the cutoff wavenumbers can be defined in this case from the panel characteristics (Bonness et al., 2010; Hambric et al., 2004);

- the last one consists in interpreting the random excitation of the WPF as a set of uncorrelated wall plane waves (UWPW) and to synthesize different realizations of the wall pressure field from an analytical formula (Maxit, 2016). This one depends on the amplitudes of the wall plane waves that are directly related to the WPF spectrum expressed in the frequency-wavenumber domain. The wall pressure fields are used as loading of the vibroacoustic model of the panel. The panel response is then deduced by averaging the responses to the different realizations of the WPF (Karimi et al., 2020a,b).

In the present paper, we propose to extend the UWPW technique for the non-homogeneous flow. Compared to the spatial and wavenumber approaches, this one has the advantage that it can be easily used in standard element-based codes (Karimi et al., 2020a) while saving computing time (Maxit et al., 2015). The process for synthesizing the WPF for non-homogeneous TBL will be based, in a primary version, on the same assumptions that the sub-area decomposition technique (SDT) (Guillon et al., 2021). The excited surface of the panel will be decomposed in different sub-areas. For each sub-area, the WPF will be estimated independently of the other sub-areas considering the superposition of uncorrelated wall plane waves. In an advanced version, the phase of the uncorrelated wall plane waves will be unchanged from one sub-area to another, that will permit to describe the correlations between the different sub-areas. The proposed technique will be compared on a test case to the spatial and the wavenumber methods that have been extended recently to non-homogeneous TBL excitation (Guillon et al., 2021).

The paper is organized as follows:

- the section 2 reminds the principle of the three methods evoked previously (i.e. spatial, wavenumber and UWPW) in the case of a homogeneous TBL excitation;

- then, the section 3 deals on the extension of these methods to the non-homogeneous TBL. First, the principles of the spatial approach and the wavenumber approach, called the sub-

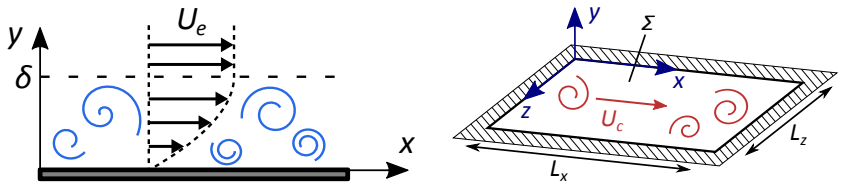

Figure 1: Rectangular baffled panel excited by a homogeneous TBL.

area decomposition technique (SDT) (Guillon et al., 2021) are presented. Then, the theoretical framework of the extension of the UWPW method is proposed in order to take the spatial variations of the TBL into account.

- the section 4 concerns the numerical applications and the comparisons of these different methods in the case of a growing TBL. Interests and limitations of these approaches are discussed before to conclude.

2. Reminder of different formulations for a panel excited by a homogeneous TBL

In this section, we consider a baffled elastic panel excited by a stationary and homogeneous TBL as schematically represented in the Fig. 1. For simplicity of the presentation, the panel of area Σ is supposed rectangular, in the plane $(\vec{x}, \vec{z})$, of length L_x and width L_z. The flow goes in the direction $\vec{x}$ at the external flow speed U_e. The TBL thickness and the convective speed are noted δ and U_c, respectively. A weak coupling is assumed between the panel and the TBL, which means that panel vibrations do not interfere with the turbulent flow. The wall pressure field induced by the TBL is characterized by the WPF cross-spectrum Ψ_{pp}, which is supposed to be known from the TBL parameters (i.e. input data of the calculation). The panel response to be estimated from the WPF cross-spectrum will be characterized by auto-spectrum density (ASD) of the panel velocity at point $\mathbf{X} \in \Sigma$. In the next three subsections, we remind the theoretical background for predicting this response with three different approaches: the spatial, the wavenumber and the UWPW approaches.

2.1. Spatial formulation

Let $\mathbf{X}$ be a point on the surface Σ and v the velocity response of the plate at this point. The auto-spectrum of the plate velocity v is given by Strawderman (1969); Maury et al. (2002):

$$S_{vv}(\mathbf{X},\omega) = \iint_{\Sigma}\iint_{\Sigma} H_v(\mathbf{X},\tilde{\mathbf{x}},\omega)\Psi_{pp}(\tilde{\mathbf{x}},\tilde{\tilde{\mathbf{x}}},\omega)H_v^*(\mathbf{X},\tilde{\tilde{\mathbf{x}}},\omega)\mathrm{d}\tilde{\mathbf{x}}\mathrm{d}\tilde{\tilde{\mathbf{x}}}, \tag{1}$$

where $H_v(\mathbf{X},\tilde{\mathbf{x}},\omega)$ is the panel FRF in velocity at point $\mathbf{X}$ for a normal unit force applied at point $\tilde{\mathbf{x}}$ and $\Psi_{pp}(\tilde{\mathbf{x}},\tilde{\tilde{\mathbf{x}}},\omega)$ is the space-frequency WPF cross-spectrum.

Semi-empirical models of the WPF spectrum have been established for flat surfaces and fully developed homogeneous TBL, where statistical properties of the pressure field are independent of the position. Hence, the WPF cross-spectrum for homogeneous TBL, Ψ_{pp}^h only depends on the space separation $\tilde{\tilde{\mathbf{x}}} - \tilde{\mathbf{x}}$ and can be written on the form (Bull, 1996):

$$\Psi_{pp}^h(\tilde{\tilde{\mathbf{x}}} - \tilde{\mathbf{x}},\omega) = \Gamma_{pp}(\tilde{\tilde{\mathbf{x}}} - \tilde{\mathbf{x}},\omega)S_{pp}(\omega), \tag{2}$$

where $\Gamma_{pp}(\tilde{\tilde{\mathbf{x}}} - \tilde{\mathbf{x}}, \omega)$ is the spatial coherence function of the separation $\tilde{\tilde{\mathbf{x}}} - \tilde{\mathbf{x}}$ and $S_{pp}(\omega)$ is the WPF auto-spectrum.

Assuming that $\forall(\tilde{\mathbf{x}},\ \tilde{\tilde{\mathbf{x}}}) \in \Sigma^2, \Psi_{pp}(\tilde{\mathbf{x}}, \tilde{\tilde{\mathbf{x}}}, \omega) = \Psi^h_{pp}(\tilde{\tilde{\mathbf{x}}} - \tilde{\mathbf{x}}, \omega)$, Eq. (1) leads to:

$$S_{vv}(\mathbf{X}, \omega) = \iint_{\Sigma} \iint_{\Sigma} H_v(\mathbf{X}, \tilde{\mathbf{x}}, \omega) \Psi^h_{pp}(\tilde{\tilde{\mathbf{x}}} - \tilde{\mathbf{x}}, \omega) H_v^*(\mathbf{X}, \tilde{\tilde{\mathbf{x}}}, \omega) \mathrm{d}\tilde{\mathbf{x}} \mathrm{d}\tilde{\tilde{\mathbf{x}}}. \tag{3}$$

Excepted for academic panels (such as simply supported rectangular panel), the FRFs appearing in this equation cannot be obtained analytically. Usually, the integrals are then replaced by discrete sums and the FRFs between the different grid points are evaluated by a numerical approach.

2.2. Wavenumber formulation

The wavenumber formulation is based on the use of the spatial Fourier transform of the WPF spectrum. Indeed, the wavenumber-frequency spectrum $\Phi^h_{pp}(\mathbf{k}, \omega)$ is defined by:

$$\Phi^h_{pp}(\mathbf{k}, \omega) = \iint_{\infty} \Psi^h_{pp}(\tilde{\tilde{\mathbf{x}}} - \tilde{\mathbf{x}}, \omega) e^{j(\tilde{\tilde{\mathbf{x}}} - \tilde{\mathbf{x}}) \cdot \mathbf{k}} \mathrm{d}\tilde{\mathbf{x}} \mathrm{d}\tilde{\tilde{\mathbf{x}}}, \tag{4}$$

where $j^2 = -1$.

Introducing this equation in Eq. (3) leads to the formulation in the wavenumber domain:

$$S_{vv}(\mathbf{X}, \omega) = \frac{1}{4\pi^2} \iint_{\infty} \left| \hat{H}_v(\mathbf{X}, \mathbf{k}, \omega) \right|^2 \Phi^h_{pp}(\mathbf{k}, \omega) \mathrm{d}\mathbf{k}, \tag{5}$$

where $\hat{H}_v(\mathbf{X}, \mathbf{k}, \omega)$ is called the velocity sensitivity function (SF). It corresponds to the velocity response at $\mathbf{X}$ when the panel is excited by a wall plane wave of wavenumber $\mathbf{k}$ (see Marchetto et al. (2018) for further details).

To integrate Eq. (5), the infinite space must be truncated with the cutoff wavenumber $\bar{k}$ and discretized. The set of wavevectors $\Omega_{\mathbf{k}}$ is bounded by $-\bar{k}$ and $+\bar{k}$ in both directions (i.e. the streamwise and transverse directions) and regularly discretized with the wavenumber step δk. The integral is then approximated and the velocity ASD becomes:

$$S_{vv}(\mathbf{X}, \omega) = \frac{1}{4\pi^2} \sum_{\mathbf{k} \in \Omega_{\mathbf{k}}} \left| \hat{H}_v(\mathbf{X}, \mathbf{k}, \omega) \right|^2 \Phi^h_{pp}(\mathbf{k}, \omega) \delta k^2. \tag{6}$$

For frequencies well above the aerodynamic coincidence frequency, the panel can generally be seen as a low-wavenumber filter and the convective contributions of the WPF have a negligible effect on the plate response. It results that the cutoff wavenumber can be defined according to the flexural wavenumber of the plate k_f (see for instance Karimi et al. (2020b)):

$$\bar{k} = \mu k_f, \tag{7}$$

where μ is a margin parameter, typically equal to 1.3. Otherwise, the convective peak of the WPF spectrum should be included in $\Omega_{\mathbf{k}}$ with a $\bar{k}$ higher than the convective wavenumber k_c.

2.3. Uncorrelated wall planes waves method

The UWPW method consists in generating different realizations of the WPF induced by the TBL and to use them as loadings of a vibroacoustic model, typically a FEM model (Maxit, 2016; Karimi et al., 2020a,b). The pressure fields are synthetized by considering a set of uncorrelated wall plane waves mimicking the TBL. The process related to this approach can be decomposed in 3 steps (Maxit, 2016):

(i) N_r realizations of the UWPW field are generated. For each realization r, the blocked pressure is calculated at the nodes $\mathbf{X} \in \Sigma$ of the FEM mesh:

$$p_b^r(\mathbf{X},\omega) = \sum_{\mathbf{k}\in\Omega_\mathbf{k}} \sqrt{S_{A_\mathbf{k}A_\mathbf{k}}(\omega)}\exp\left\{j\left(\mathbf{k}\cdot\mathbf{X}+\varphi_\mathbf{k}^r\right)\right\}, \tag{8}$$

where $\varphi_\mathbf{k}^r$ are random phases uniformly distributed in $[0;2\pi]$ expressing the fact that the waves are uncorrelated and the wave amplitude auto-spectrum is given by:

$$S_{A_\mathbf{k}A_\mathbf{k}}(\omega) = \frac{\Phi_{pp}^h(\mathbf{k},\omega)\delta k^2}{4\pi^2}; \tag{9}$$

(ii) the panel response at node $\mathbf{X}$ in velocity to the r-th realization of the synthesized WPF, noted $v^r(\mathbf{X},\omega)$, is computed with the vibroacoustic model. The process is iterated for all realizations $r \in [\![1, N_r]\!]$;

(iii) the velocity auto-spectrum at $\mathbf{X}$ in response to the TBL excitation is the ensemble average of the responses $v^r(\mathbf{X},\omega)$ for $r \in [\![1, N_r]\!]$:

$$S_{vv}(\mathbf{X},\omega) = \mathbb{E}\left[v^r(\mathbf{X},\omega)\left(v^r(\mathbf{X},\omega)\right)^*\right]_r = \frac{1}{N_r}\sum_{r=1}^{N_r}\left|v^r(\mathbf{X},\omega)\right|^2, \tag{10}$$

where $\mathbb{E}[\cdot]_r$ is the ensemble average.

When a finite element model is considered for the panel (Karimi et al., 2020a; Maxit, 2016), the element size in the streamwise and crosswise directions, δx and δz, should respect the following criterion:

$$\delta x < \frac{\pi}{\bar{k}_x}\,,\ \delta z < \frac{\pi}{\bar{k}_z}\,. \tag{11}$$

3. Panel excited by a non-homogeneous turbulent boundary layer

The methods for predicting the vibrational response of a panel for a homogeneous excitation have been given in the previous section. In the following, the TBL is no longer spatially homogeneous. A typically case that will be considered for the numerical applications is the growing of a fully turbulent boundary layer triggered at one edge (for instance with a sand paper strap), as schematically represented in Fig. 2. For such case, the laminar and transition regions are supposed small compared to the plate surface. That permits to approximate the TBL as fully turbulent over all the plate surface. Using some hypotheses, the previous methods can be adapted to estimate the panel response to these non-homogeneous excitations. It was the purpose of the work presented in (Guillon et al., 2021) for the spatial and the wavenumber approaches. We are going to remind the main results for these two approaches before to extend the UWPW method, that constitutes the novelty of the present paper. The results predicted by the different approaches will be compared and discussed in the section 4.

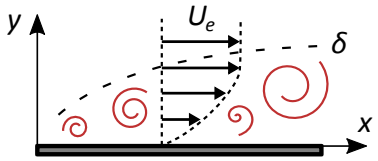

Figure 2: Spatially varying TBL along stream direction $\vec{x}$.

3.1. Spatial formulation

Eq. (1) can be used to evaluate the panel response to a non-homogeneous excitation. However, the difficulty to apply this formula relies on the estimation of the cross-spectrum of WPF, $\Psi_{pp}(\tilde{\mathbf{x}}, \tilde{\tilde{\mathbf{x}}}, \omega)$, for all the couple of points on the plate, $(\tilde{\mathbf{x}}, \tilde{\tilde{\mathbf{x}}}) \in \Sigma^2$. However, the WPF of a TBL is weakly correlated spatially. The coherence length Λ is an indicator of the decay of the spatial correlation of the pressure field. For two points whose separation distance is small compared to the coherence length, it can be assumed that the TBL presents small variations and that the WPF could be approximated by considering a local homogeneous TBL. When the separation becomes large compared to the coherence length, the correlation tends to zero. Under these simplifying assumptions, the cross-spectrum of the WPF between $\tilde{\mathbf{x}}$ and $\tilde{\tilde{\mathbf{x}}}$ can be approximated by (Guillon et al., 2021):

$$\Psi_{pp}(\tilde{\mathbf{x}}, \tilde{\tilde{\mathbf{x}}}, \omega) \approx \begin{cases} \left[S_{pp}(\omega) \Gamma_{pp}(\tilde{\tilde{\mathbf{x}}} - \tilde{\mathbf{x}}, \omega) \right]_{\tilde{\mathbf{x}}, \tilde{\tilde{\mathbf{x}}}} & \text{if } \|\tilde{\tilde{\mathbf{x}}} - \tilde{\mathbf{x}}\| < 4\Lambda(\omega), \\ 0 & \text{if } \|\tilde{\tilde{\mathbf{x}}} - \tilde{\mathbf{x}}\| \geqslant 4\Lambda(\omega), \end{cases} \tag{12}$$

where Λ is the coherence length of the WPF and the quantities S_{pp} and Γ_{pp} are calculated using the arithmetic mean of TBL parameters at $\tilde{\mathbf{x}}$ and $\tilde{\tilde{\mathbf{x}}}$.

It is important to note that the spatial method is not valid for low frequencies. Indeed, the Corcos model predicts a ω^{-1} decay rate of the coherence length which has been verified experimentally (Salze et al., 2014). In the low frequency range, the coherence length is large and it can then be of the same order than the length of the panel. The assumption of a local homogeneous TBL cannot be applied. In contrary, in the mid and high frequencies, the coherence length is much smaller compared to the length of the panel and the assumption of a local homogeneous TBL model can be applied when the TBL parameters do not vary significantly along a coherence length. In the following, the scope will be focused on frequencies where the coherence is at least two times smaller than the panel length.

3.2. Wavenumber formulation: sub-area decomposition technique

Supposing the spatially homogeneous excitation in Eq. (3) and introducing the space Fourier transform allowed us to propose the wavenumber formulation in section 2.2. This mathematical operation can obviously not be performed directly in Eq. (1) for a spatially varying TBL. Nevertheless, the panel surface Σ can be divided into N sub-areas along the streamwise direction $\vec{x}$. Then a locally homogeneous TBL is assumed on each sub-area, as shown in Fig. 3. Eq. (1) can be rewritten:

$$S_{vv}(\mathbf{X}, \omega) = \sum_{p=1}^{N} \sum_{q=1}^{N} \iint_{\tilde{\mathbf{x}} \in \Sigma_p} \iint_{\tilde{\tilde{\mathbf{x}}} \in \Sigma_q} H_v(\mathbf{X}, \tilde{\mathbf{x}}, \omega) \Psi_{pp}(\tilde{\mathbf{x}}, \tilde{\tilde{\mathbf{x}}}, \omega) H_v^*(\mathbf{X}, \tilde{\tilde{\mathbf{x}}}, \omega) \mathrm{d}\tilde{\mathbf{x}} \mathrm{d}\tilde{\tilde{\mathbf{x}}}. \tag{13}$$

Eq. (13) contains $N \times N$ terms, with N the number of sub-areas. The equation may be made simpler, as some terms can be neglected considering the properties of the WPF:

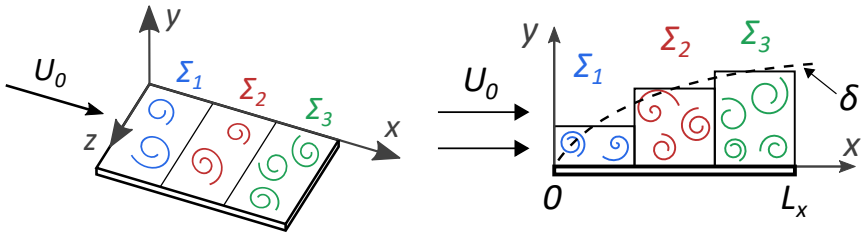

Figure 3: Sub-area discretization of Σ.

- on one side, for two points belonging to the same sub-area, TBL parameters are assumed constant and a cross-spectrum for a homogeneous excitation can be used;
- on the other side, the spatial correlation is a decreasing function of the two points spatial separation. It is assumed that, when the two points belong to distinct sub-areas, their spatial separation is high compared to the coherence length so that their correlation is negligible.

Following these assumptions, a growing TBL is approximated by the sequence of homogeneous TBL as illustrated on Fig. 3 for 3 sub-areas.

These assumptions can be translated into the following equation:

$$(\tilde{\mathbf{x}},\ \tilde{\tilde{\mathbf{x}}}) \in \left(\Sigma_p \times \Sigma_q\right),\ \Psi_{pp}(\tilde{\mathbf{x}},\tilde{\tilde{\mathbf{x}}},\omega) = \begin{cases} \Psi_{pp}^{h,\zeta}(\tilde{\tilde{\mathbf{x}}}-\tilde{\mathbf{x}},\omega) & \text{if } p = q = \zeta, \\ 0 & \text{if } p \neq q, \end{cases} \tag{14}$$

with $\Psi_{pp}^{h,\zeta}$ is the cross-spectrum of the WPF for a homogeneous load, attributed to the sub-area ζ which is estimated considering an arithmetic mean of TBL parameters on surface Σ_ζ.

It results that each sub-area ζ of surface Σ_ζ is associated with a locally homogeneous spectrum. Introducing Eq. (14) into Eq. (13), only the terms $p = q$ remain. It is then possible to define the wavenumber-frequency cross-spectrum $\Phi_{pp}^{h,\zeta}(\mathbf{k},\omega)$ of the sub-area ζ as the Fourier transform of $\Psi_{pp}^{h,\zeta}(\tilde{\tilde{\mathbf{x}}}-\tilde{\mathbf{x}},\omega)$. Finally, the velocity auto-spectrum can be written (Guillon et al., 2021):

$$S_{vv}(\mathbf{X},\omega) = \frac{1}{4\pi^2}\sum_{\zeta=1}^{N}\sum_{\mathbf{k}\in\Omega_\mathbf{k}} \left|\hat{H}_v^\zeta(\mathbf{X},\mathbf{k},\omega)\right|^2 \Phi_{pp}^{h,\zeta}(\mathbf{k},\omega)\delta k^2, \tag{15}$$

where $\hat{H}_v^\zeta(\mathbf{X},\mathbf{k},\omega)$ is the plate response in velocity at $\mathbf{X}$ when the panel is excited by a wall plane wave on surface Σ_ζ.

This approach has been called the sub-area decomposition technique (SDT). With the SDT, because of the spatial correlation of the WPF, the length of the sub-area needs to respect a criterion related to the cutoff wavenumber (Guillon et al., 2021):

$$\frac{L_x}{N} \geqslant \frac{3}{2}.\frac{2\pi}{\bar{k}}. \tag{16}$$

Moreover, the SDT is valid when the convective wavenumber k_c is significantly greater than the flexural wavenumber k_f. Under this condition, it is assumed that the convective peak has a weak role in the vibrational panel response and that it can be neglected. Therefore, the convective peak can be filtered out of the integration domain, according to Eq. (7).

3.3. Uncorrelated wall planes waves applied to the sub-area decomposition

In this subsection, the UWPW method is extended to calculate the panel response to non-homogeneous TBL excitations. The same principle than the SDT described previously is considered at first. The excited surface of the panel is decomposed in N sub-areas and a wavenumber-frequency cross-spectrum $\Phi_{pp}^{h,\zeta}(\mathbf{k},\omega)$ is associated to each sub-area $\zeta \in [\![1,N]\!]$ (as in the previous section). Moreover, in a first approach and as for the SDT, the pressures acting on two different sub-areas are supposed to be uncorrelated (as expressed by Eq. (14)). The pressure field can then be determined on each sub-area, separately. This pressure field should correspond to the one of a locally homogeneous TBL characterized by the cross-spectrum $\Phi_{pp}^{h,\zeta}(\mathbf{k},\omega)$ in the sub-area ζ. The Eq. (8) defining the blocked pressure for a homogeneous TBL can be reused for defining the blocked pressure related to the sub-area ζ. The cross-spectrum of the WPF related to the sub-area ζ should be considered. The random phases occurring in Eq. (8) have be chosen different from one sub-area to another due to the fact that the pressures acting on different sub-areas are uncorrelated. These random phases are noted ${}^{\zeta}\varphi_{\mathbf{k}}^{r}$, where we remind that $\mathbf{k}, r, \zeta$ are, respectively, the wall plane wave index, the realization index, and the sub-area index.

The blocked pressure on the sub-area $\zeta \in [\![1,N]\!]$ can then be expressed by:

$$\mathbf{X} \in \Sigma_\zeta\,, \quad p_b^r(\mathbf{X},\omega) = \sum_{\mathbf{k}\in\Omega_{\mathbf{k}}} \sqrt{S_{A_{\mathbf{k}}^\zeta A_{\mathbf{k}}^\zeta}(\omega)}\exp\left\{j\left(\mathbf{k}\cdot\mathbf{X} + {}^{\zeta}\varphi_{\mathbf{k}}^{r}\right)\right\}, \tag{17}$$

$$\text{with} \quad S_{A_{\mathbf{k}}^\zeta A_{\mathbf{k}}^\zeta}(\omega) = \frac{\Phi_{pp}^{h,\zeta}(\mathbf{k},\omega)\delta k^2}{4\pi^2}. \tag{18}$$

Realizations of the wall pressure field can be generated using this formula for the different sub-areas. As for the homogeneous excitation, the WPF can be introduced as loads in the panel vibratory model to deduce the panel response. An ensemble average on the panel response to the different realizations is then performed to estimate the panel response to the non-homogeneous TBL. The synthesis of these WPF by this process supposes that the pressures acting on distinct sub-areas are uncorrelated. This approach named the "local" uncorrelated wall plane wave (L-UWPW) technique is equivalent to the SDT method and should give the same predictions.

For the SDT, the decorrelation of the WPF spectrum between the different sub-areas is a mandatory condition to perform a spatial Fourier transform. However, with the UWPW method, this condition can be easily relaxed by taking the same phases, $\varphi_{\mathbf{k}}^{r}$, for the different sub-areas. This supposes that the wall plane waves are defined globally on the whole excited surface, but their amplitudes can vary from one sub-area to another. Under this condition (i.e. ${}^{\zeta}\varphi_{\mathbf{k}}^{r} = \varphi_{\mathbf{k}}^{r}$, for $\zeta \in [\![1,N]\!]$) the wall pressure field of the realization r is given by:

$$\mathbf{X} \in \Sigma_\zeta\,, \quad p_b^r(\mathbf{X},\omega) = \sum_{\mathbf{k}\in\Omega_{\mathbf{k}}} \sqrt{S_{A_{\mathbf{k}}^\zeta A_{\mathbf{k}}^\zeta}(\omega)}\exp\left\{j\left(\mathbf{k}\cdot\mathbf{X} + \varphi_{\mathbf{k}}^{r}\right)\right\}. \tag{19}$$

As the wall plane waves are defined on the global scale of the panel, it is name the "global" uncorrelated wall plane wave (G-UWPW) technique.

We have presented two alternative approaches to take the spatial variations of the TBL parameters into account in the UWPW method. In the next section, we are going to assess the validity of these two approaches by comparing their results to the ones obtained both by the spatial approach and the SDT, that we have described in the sections 3.1 and 3.2, respectively. We will also present a third version of the extension of the UWPW method for a non-homogeneous TBL.

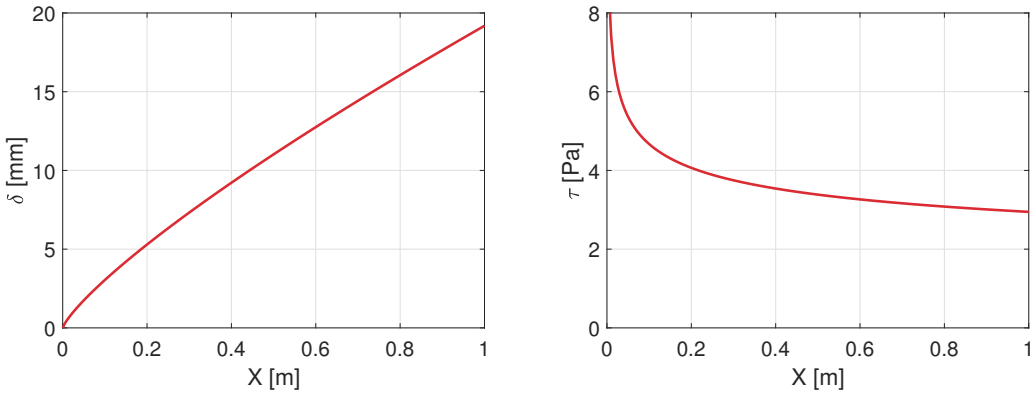

(a) (b)

Figure 4: TBL parameters estimated from Eq. (20) and Eq. (21).
(a): TBL thickness δ; (b): shear stress τ. Free stream velocity: 40 m/s.

4. Numerical applications

4.1. Turbulent boundary layer parameters

The 1 meter long and 0.35 meter large rectangular panel shown in Fig. 2 is set in a flow of free stream velocity equal to 40 m/s, $\vec{x}$ corresponding to the streamwise direction. The TBL is supposed triggered by a sandpaper strip at the plate edge $x = 0$. The TBL parameters will be estimated with an analytical model for a flat smooth plate (Sanders, 2014). This model for 2-D $(\vec{x}, \vec{y})$ incompressible flow supposes a zero pressure gradient and external velocity U_e constant and equal to the free stream velocity. Moreover, the laminar and transitional regions are neglected. Under these assumptions, the TBL thickness and the shear stress can be estimated by (Sanders, 2014; Schilchting and Gersten, 2017):

$$\delta = 0.37 \left(\frac{\nu}{U_e} \right)^{1/5} x^{4/5}, \tag{20}$$

$$\tau = \frac{1}{2} \rho U_e^2 \, 0.0592 \left(\frac{\nu}{U_e x} \right)^{1/5}. \tag{21}$$

The TBL parameters estimated with this model are plotted on Fig. 4. The TBL thickness increases along the length of the plate, whereas the shear stress decreases significantly along the first third of the length of the plate and then remains roughly constant. Considering an arithmetic average of these quantities, 10.7 mm is obtained for the TBL thickness and 3.76 Pa for the shear stress. These averaged values would be the ones considered if the TBL would be supposed homogeneous (as it will be the case in the section 4.6 for comparison).

In the following, the Goody model (Goody, 2004) will be considered for the auto-spectrum of the WPF whereas the Mellen model (Mellen, 1990) will be considered for the normalized cross-spectrum. Hence, the wavenumber-frequency cross-spectrum of the WPF will be estimated by:

$$\Phi_{pp}(k_x, k_z, \omega) = S_{pp}(\omega) . \frac{2\pi \alpha_x^2 \alpha_z^2 k_c}{\left((\alpha_x \alpha_z k_c)^2 + (\alpha_x k_z)^2 + \alpha_z^2 (k_x - k_c)^2 \right)^{3/2}} \tag{22}$$

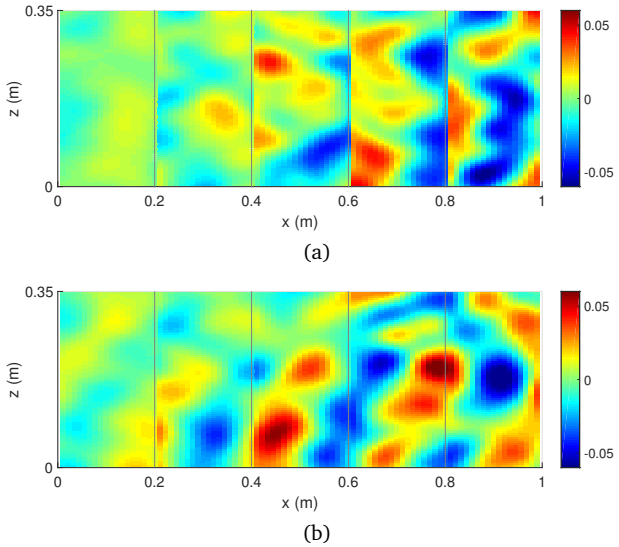

Figure 5: Two examples of realization of the pressure field (Pa) at 100 Hz;
(a): L-UWPW method; (b): G-UWPW method.
Black vertical lines indicate the sub-area boundaries.

with:

$$S_{pp}(\omega) = \frac{\delta\tau^2}{U_e} \cdot \frac{c_2(\omega\delta/U_e)^2}{\left[(\omega\delta/U_e)^{0.75} + c_1\right]^{3.7} + \left[c_3((\delta/U_e)/(\rho\nu/\tau))^{-0.57}(\omega\delta/U_e)\right]^7}, \tag{23}$$

where $c_1 = 0.5$, $c_2 = 3$, $c_3 = 1.1$, $\alpha_x = 0.10$, $\alpha_z = 0.77$ and $k_c = \omega/U_c$ is the convective wavenumber.

4.2. *Pressure fields synthetized with the L-UWPW and G-UWPW methods*

Realizations of the blocked pressure p_b are calculated with Eq. (17) and Eq. (19), corresponding to the L-UWPW and G-UWPW methods, respectively. One realization for each method is shown in the $(\vec{x}, \vec{z})$ plane at 100 Hz on Fig. 5, when considering 5 sub-areas.

Fig. 5(a) corresponds to the L-UWPW method. The intensity of the pressure field is increasing in the streamwise direction, which is consistent with the growing of the TBL. However, some discontinuities of the pressure field can be clearly observed at the sub-area boundaries. Independent random wall plane wave phases ${}^{\zeta}\varphi^{r}_{\mathbf{k}}$ have been considered in order to simulate uncorrelated pressure fields from one sub-area to another as in the SDT (Guillon et al., 2021). This assumption has been useful for establishing the formulation, but the discontinuities observed resulting of this assumption are not representative of the TBL pressure fluctuations.

On the other hand, Fig. 5(b) shows the results for the G-UWPW method that supposes identical wall plane wave phases for the different sub-areas. The resulting pressure field is spatially continuous, even through the sub-area boundaries, that is consistence with the physic of the TBL. The intensity of the pressure is still increasing along the $\vec{x}$ axis.

In order to further assess the pressure synthesized with the two proposed methods, an ensemble of N_r realizations are used to calculate the auto-spectrum of the synthesized pressure field $S_{p_b p_b}$

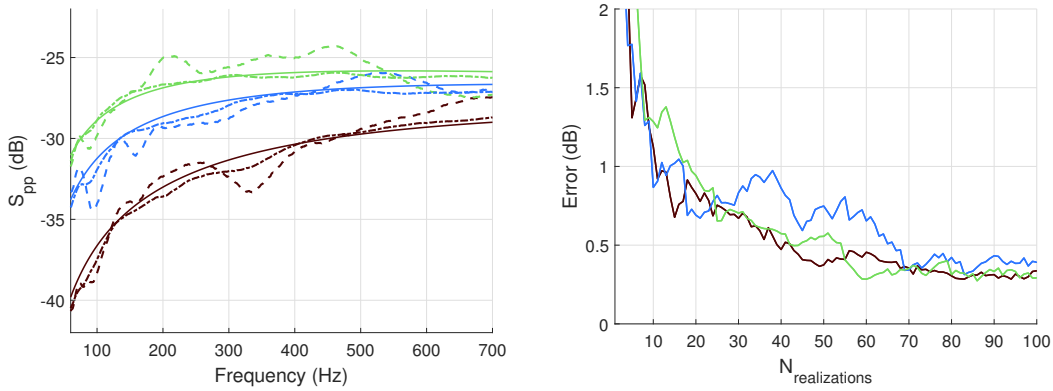

Figure 6: Analysis of the synthesized pressure field at 3 points: green $x = 0.2L_x$, blue $x = 0.5L_x$, brown $x = 0.8L_x$. (a): Auto-spectrum for the synthesized pressure field (dB, ref. $1\,\mathrm{Pa}^2/\mathrm{Hz}$). Three calculations (G-UWPWP): dashed line, 20 realizations; dash-dot line, 200 realizations; continuous line, analytical with Goody model (reference). (b): Average in the frequency band [50 - 700] Hz of the absolute errors between the G-UPWP prediction and the Goody model in function of the number of realizations.

at a point $\mathbf{X}$, with the following equation:

$$S_{p_b p_b}(\mathbf{X},\omega) = \mathbb{E}\left[p_b^r(\mathbf{X},\omega)\left(p_b^r(\mathbf{X},\omega)\right)^*\right]_r. \tag{24}$$

The estimated auto-spectrum considering the blocked pressure calculated with Eq. (19), for three different positions along $\vec{x}$ axis, is plotted in Fig. 6(a) and compared to the auto-spectrum of the Goody model from Eq. (23). Since only the information at the point $\mathbf{X}$ is relevant, the L-UWPW and the G-UWPW methods display the same prediction. The difference of levels for the different observation points as well as the global frequency variations are well described by the synthesized pressures. In order to inspect more in details the convergence of the process, the Fig. 6(b) shows the average absolute error on the frequency band [50, 700] Hz between the auto-spectrum of the synthesized pressure field and the Goody model, as a function of the number of realizations. It can be observed that the errors decrease globally when the number of realization increases whatever the point considered. The average error is below 1 dB above 20 realizations. Consequently, adopting a margin to guarantee an error below 1 dB, it can be presumed that the convergence is reached for 30 realizations.

Now, let us focusing on the spatial coherence of the pressure fields synthetized by the two UWPW methods as a function of the distance from a fixed observation point $\mathbf{X_0}$. The coherence is then calculated with the following formula:

$$\Gamma_{p_b p_b}(\mathbf{X_0},\mathbf{X},\omega) = \frac{\left|\mathbb{E}\left[p_b^r(\mathbf{X_0},\omega)\left(p_b^r(\mathbf{X},\omega)\right)^*\right]_r\right|}{\left(\mathbb{E}\left[\left|p_b^r(\mathbf{X_0},\omega)\right|^2\right]_r \mathbb{E}\left[\left|p_b^r(\mathbf{X},\omega)\right|^2\right]_r\right)^{1/2}}. \tag{25}$$

The spatial coherence $\Gamma_{p_b p_b}$ considering the L-UWPW method is plotted along the stream direction $\vec{x}$ on Fig. 7, at two frequencies $f = 100\,\mathrm{Hz}$ and $f = 400\,\mathrm{Hz}$ for $\mathbf{X_0} = (L_x/2; L_z/2)$. The

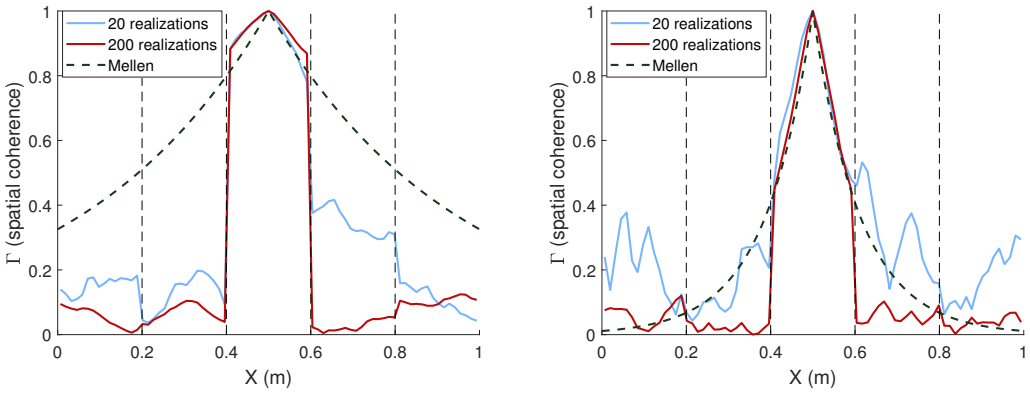

Figure 7: Spatial coherence of the pressure field synthesized by the L-UWPW method considering 5 sub-areas. (a): 100 Hz; (b): 400 Hz.

vertical dark dotted lines indicate the sub-areas boundaries and the dotted curve corresponds to the exponential decay of the Mellen model given by:

$$\Gamma_{pp}(\mathbf{X_0}, \mathbf{X}, \omega) = \exp\left\{-\alpha_x \left\|\mathbf{X} - \mathbf{X_0}\right\| k_c\right\}. \tag{26}$$

Within the sub-area containing the point $\mathbf{X_0}$, the decay of the coherence of the synthesized pressure field is in agreement with the Mellen model. However, the drop of the coherence when crossing a sub-area boundary expresses that the pressure fields applied on two different sub-areas are uncorrelated, which is not consistent with the Mellen model.

When considering the G-UWPW method, the coherence $\Gamma_{p_b p_b}$ shown on Fig. 8, is continuous even through the sub-area boundaries and globally in agreement with the decrease of the Mellen model. This agreement seems well better with 200 realizations than with 20 realizations. However, it will be seen later that the convergence of the panel vibration prediction is achieved with only 30 realizations as it was pointed out for homogeneous excitations in Maxit (2016). This can be explained by the fact that the weakly correlated contributions of the WPF have few influence on the panel response and therefore it is not necessary to predict them accurately.

4.3. Plate vibratory model

A rectangular aluminum panel simply supported on its four edges is considered for the following numerical applications. The material Young's modulus E, Poisson's ratio ν_p and mass density ρ_p are respectively, 68.9 GPa, 0.35 and $2740\,\mathrm{kg/m^3}$. The panel dimensions are 1 m and 0.35 m in the streamwise and crosswise directions, respectively. The panel thickness h linearly varies along the x-axis from 2 mm at the leading edge to 6 mm at the trailing edge as schematically represented on Fig. 9. A varying thickness has been chosen in order to stress the effect of the spatial variation of the excitation, while keeping an almost canonical case. Indeed, because of the symmetry of the modal shapes for a simply supported plate with constant thickness, the influence of the spatial evolution of the TBL on the vibration behavior is flattened. This symmetry of the mode shapes is broken when considering a variation of the thickness in the streamwise direction, the modes can then be excited with different strengths depending on the spatial distribution of the loadings due

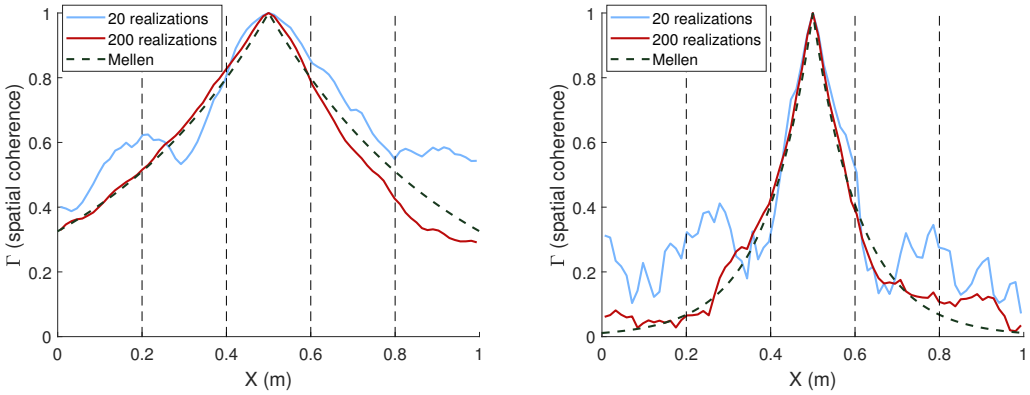

Figure 8: Spatial coherence of the pressure field synthesized by the G-UWPW method with 5 sub-areas. (a): 100 Hz; (b): 400 Hz.

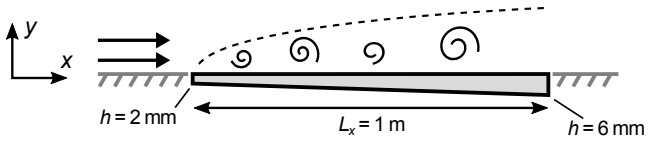

Figure 9: 2-D panel view (width $L_z = 0.35\,\mathrm{m}$).

to the TBL. It is assumed that the slope resulting from this spatial variation of the thickness is weak and does not affect the TBL compared to a flat panel.

The normal modes of the undamped panel have been extracted from a finite element model using the MSC NASTRAN software. Two 2-D meshes composed of quadrilateral linear elements (CQUAD4) have been considered:

- the coarser one is composed of 2759 nodes: 89 along $\vec{x}$ and 31 along $\vec{z}$. This mesh is adapted for the UWPW and SDT calculations that considered wall pressure fields filtered at a given cutoff wavenumber $\bar{k}$. The element-size criterion defined by Eq. (11) is respected even when the cutoff wavenumber in the streamwise direction is defined regarding the convective wavenumber. This will make it possible to perform UWPW calculations including the convective contributions even if in general they will have a negligible effect on the vibrations of the panel;

- the finer one, composed of 29344 nodes: 131 along $\vec{x}$ and 224 along $\vec{z}$. This mesh is adapted for the spatial calculations. It permits to describe the variations of the WPF due to the flow convection as well as the small coherence length of the WPF in the transverse direction. Indeed, the mesh exhibits 5 elements per convective wavelength in the $\vec{x}$ direction and 5 elements per coherence length in the $\vec{z}$ direction at the highest frequency of interest.

Shell properties (PSHELL) and isotropic material properties (MAT1) have been used. Respective thicknesses are assigned at the four nodes of each quadrilateral element for describing the plate thickness variations. The plate modes are extracted with a normal modal analysis using the Lanczos method (SOL103) up to 1000 Hz. The vibratory responses of the panel induced by the WPF have

then been estimated using the modal expansion technique with a damping loss η factor set at 1% for all the modes.

4.4. Comparison of the vibratory response prediction

Let us compare the plate velocity response predicted by the different methods presented in the section 3. The flow conditions considered in these calculations are the ones presented in the section 4.1. In particular, the flow speed is 40 m/s and the TBL parameters vary spatially according to Fig. 4.

The SDT method and the L-UWPW method, that both consider uncorrelated pressure fields on the different sub-areas, are compared in Fig. 10(a) in terms of spatial mean square velocity of the plate:

$$\bar{S}_{vv}(\omega) = \frac{1}{\Sigma} \iint_{\Sigma} S_{vv}(\mathbf{X}, \omega) \mathrm{d}\mathbf{X}. \tag{27}$$

The vibratory calculations were achieved considering 5 sub-areas and using 10 realizations of the pressure field for the L-UWPW method. The choice of the number of sub-areas have been the subject of a discussion in Guillon et al. (2021). Increasing the number of sub-areas leads to a better representation of the continuous growth of the TBL, at the cost of the loss of global spatial correlation of the excitation, in particular for the formulation with uncorrelated sub-areas used here. When the convective peak is filtered, a suggested criterion based on the cutoff wavenumber is given in Eq. (16). Frequency range starts at 100 Hz, where the coherence length Λ is at least two times smaller than the panel length. As expected, both methods give very similar results. Fig. 10(b) shows the difference of prediction between the L-UWPW method and the SDT for different number of realizations. It can be observed that higher is the number of realizations in the L-UWPW method, lower is the discrepancy between the two methods. An average of these discrepancies over the studied frequency range gives 0.76 dB with 10 realizations, 0.41 dB with 30 realizations and it goes down to 0.18 dB with 100 realizations. In the following, 30 realizations will be used for the computation of the pressure field with UWPW methods.

Now, the results of the L-UWPW and G-UWPW methods are compared with the ones of the spatial method that can be seen as a reference. The discrepancies of the prediction between the two UWPW approaches and the spatial approach are shown in Fig. 11 in function of the frequency. Overall, the differences with the spatial approach are similar for the two UWPW approaches for the frequencies above the third mode, that is to say above 159 Hz. Average error comparing the spatial method for the L-UWPW method is 0.62 dB whereas it is 0.61 dB with the G-UWPW method in the frequency range [159-700] Hz. At some frequencies close to the resonance frequencies, the differences can be more significant (around 1 or 2 dB) with a change of sign at the resonances. This can be explained by a shift of the resonant frequencies predicted by using two different meshes (i.e. the coarser mesh for the UWPW calculations and the finer one for the spatial calculation). The C-UWPW processes are then not directly at the origin of these discrepancies. A supplementary C-UWPW calculation have been performed considering the modal frequencies calculated by FEM with the finer mesh. In this case, the differences between the C-UWPW and the spatial results are less than 1 dB over all the frequency range (result not shown). The differences observed in Fig. 11 can then be attributed to discrepancies in the modal frequencies predictions with the two meshes and not to the accuracy of the C-UWPW approach. Nonetheless, the L-UWPW predictions diverge in the low frequencies. This result could be expected as the L-UWPW approach supposes, as SDT, that the pressure fields acting on the different sub-areas are uncorrelated. The validity criterion on the minimum sub-area size defined by Eq. (16) that was originally defined for the SDT should also be respected for the L-UWPW method. When the frequency decreases, the flexural wavenumber

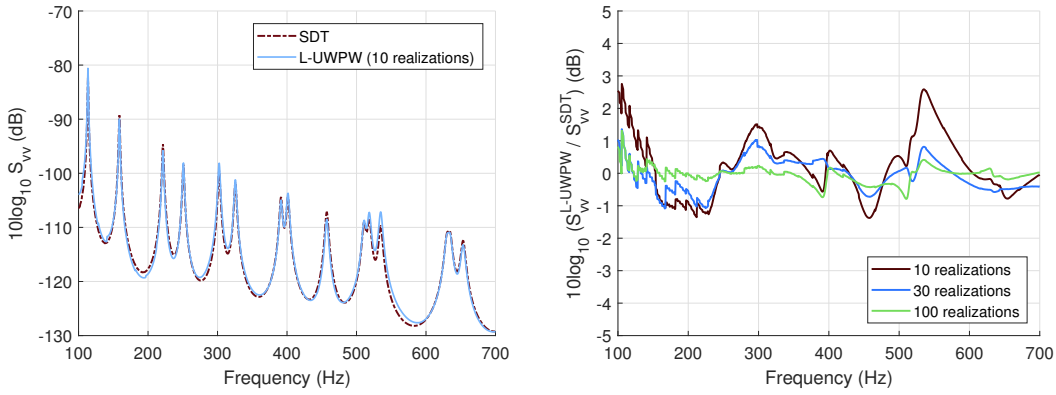

(a) (b)

Figure 10: Spatial mean square velocity predicted by the SDT and the L-UWPW method considering 5 sub-areas. (a): Velocity level (dB, ref. $1\,(\mathrm{m/s})^2/\mathrm{Hz}$). (b): Difference between the L-UWPW method and the SDT predictions for different number of realizations.

and then the cutoff wavenumber $\bar{k}$ defined by Eq. (7) decreases. This implies that fewer sub-areas must be considered in the low frequency range compared to upper frequencies in order to respect the criterion of Eq. (16). Whereas the L-UWPW approach is not well adapted for the low frequencies, one can emphasize that the G-UWPW gives accurate results in the whole frequency range as observed in Fig. 11.

As the G-UWPW approach does not consider that the pressure fields acting on different sub-areas are uncorrelated, it does not require to fulfill the criterion (16) on the minimum sub-areas sizes. An "asymptotic" formula can be then proposed by considering a number of sub-areas N equal to the number of nodes of the plate mesh, so that each node is associated to its own sub-area. The blocked pressure at node $\mathbf{X}$ can then be calculated by:

$$p_b^r(\mathbf{X},\omega) = \sum_{\mathbf{k}\in\Omega_\mathbf{k}} \sqrt{S_{A_\mathbf{k}A_\mathbf{k}}(\mathbf{X},\omega)}\exp\left\{j\left(\mathbf{k}\cdot\mathbf{X}+\varphi_\mathbf{k}^r\right)\right\}, \tag{28}$$

$$\text{with}\quad S_{A_\mathbf{k}A_\mathbf{k}}(\mathbf{X},\omega) = \frac{\Phi_{pp}^{\mathbf{X}}(\mathbf{k},\omega)\delta k^2}{4\pi^2}, \tag{29}$$

where $\Phi_{pp}^{\mathbf{X}}(\mathbf{k},\omega)$ is the WPF spectrum calculated with the TBL parameters at $\mathbf{X}$.

As the concept of sub-area decomposition does not appear explicitly in this last formulation and the pressure can vary from one node to another, the process related to Eq. (28) is named the "continuously" varying uncorrelated wall plane waves (C-UWPW) technique. For illustration, Fig. 12 presents two realizations of the WPF synthetized with the C-UWPW for the same situation than Fig. 5. The WPF varies well continuously and the strength is growing gradually from the leading edge to the trailing edge.

It can also be underlined that as the assumption consisting in neglecting the convective contributions was related to the sub-area decomposition (Guillon et al., 2021), the C-UWPW can likely describe these convective contributions when it is necessary (for instance, for frequencies below or close to the aerodynamic coincidence frequency). In order to verify that the C-UWPW calculation

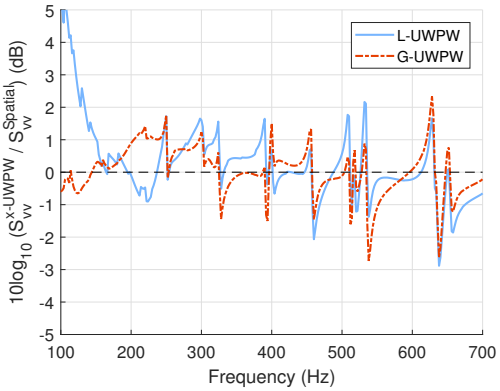

Figure 11: Difference of mean square velocity level between the spatial approach and the L-UWPW or the G-UWPW approaches. 30 realizations and 5 sub-areas.

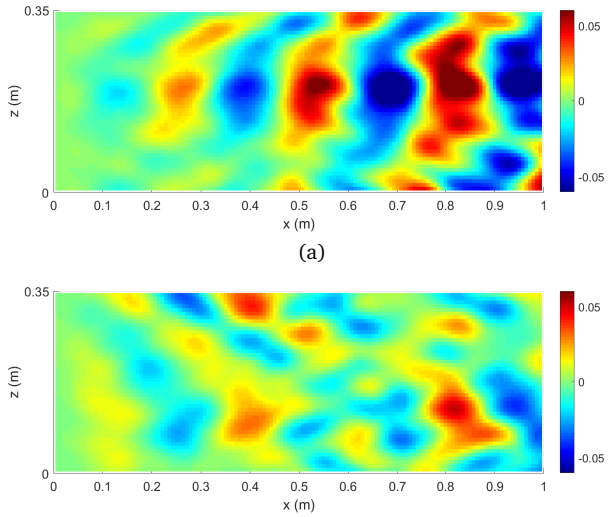

Figure 12: Two examples of realization of the pressure field (Pa) at 100 Hz generated by the C-UWPW method.

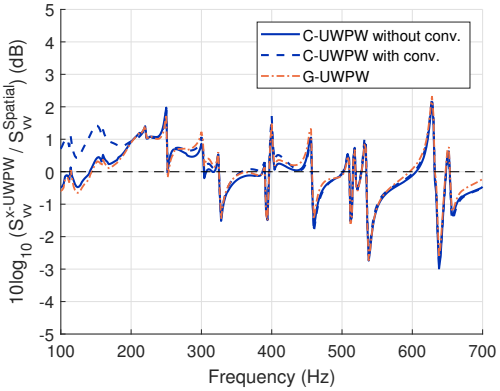

Figure 13: Difference of mean square velocity level between the spatial approach and the C-UWPW approach, with and without the convective contributions (30 realizations). Results of the G-UWPW approach from Fig. 11 added for comparison.

converges well when the convective contributions are taken into account (even if these contributions have a negligible effect on the panel vibrations), the method is applied with two different cutoff wavenumbers: first with a $\bar{k}$ defined by Eq. (7), which means that the contributions of the convective of the WPF are neglected and second with $\bar{k} = 180\,\mathrm{rad/m}$, which is higher than the maximum convective wavenumber k_c at 700 Hz, meaning that the contributions of the convective of the WPF are taken into account. The difference of prediction with the spatial approach for the C-UWPW method with and without the convective contributions are displayed in Fig. 13. First, it can be observed that the discrepancies with the spatial approach are smaller than 0.5 dB in general. As for Fig. 11, some more significant discrepancies close to the resonant frequencies can be attributed to difference of prediction of the resonant frequencies using the two different meshes. The results in Fig. 13 are then satisfying and validates the C-UWPW approach for the present case. Second, the two C-UWPW calculations match very well above 200 Hz whereas they are close to each other below this frequency. Average error regarding to the spatial method is 0.61 and 0.72 dB with 30 realizations, respectively without and with the convective contributions. This shows that taking the convective contributions do not induce a divergence of the process. However, for the present case and the frequencies considered well above the aerodynamic coincidence frequency, the effect of the convective contributions is negligible on the panel vibrations.

Finally, two realizations of the pressure field used in the G-UWPW calculation with the convective peak are displayed in Fig. 14(a) and (c) and Fig. 15(a) and (c), at two given frequencies. In Fig. 14, 159 Hz corresponds to a resonance (the third natural mode of the panel) and in Fig. 15, 277 Hz corresponds to an anti-resonance, halfway through the fifth and sixth natural modes (first natural mode is below 100 Hz). The panel velocity field resulting from each pressure field are plotted respectively in Fig. 14(b) and (d) and Fig. 15(b) and (d). For the resonance, the velocity figures show that the modal shape dominates the plate behavior for any load. At the anti-resonance, different plate responses could be observed for different pressure fields. The said responses are still summations of modal shapes.

4.5. Panel with free edges: role of the convective peak

To highlight the effect of the convective contributions in some situations and to verify the accuracy of the C-UWPW approach for such cases, let us considered a second test case. The plate

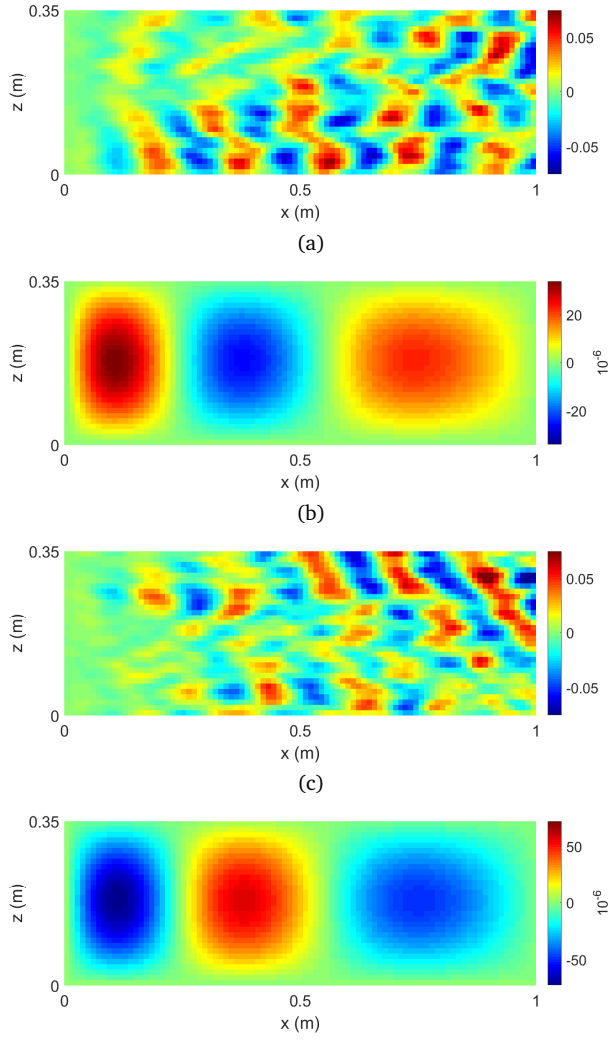

Figure 14: (a), (c): pressure fields (Pa) at the nodes of the spatial grid, generated by the C-UWPW method and (b), (d): their respective corresponding velocity fields (m/s), for a resonance (159 Hz).

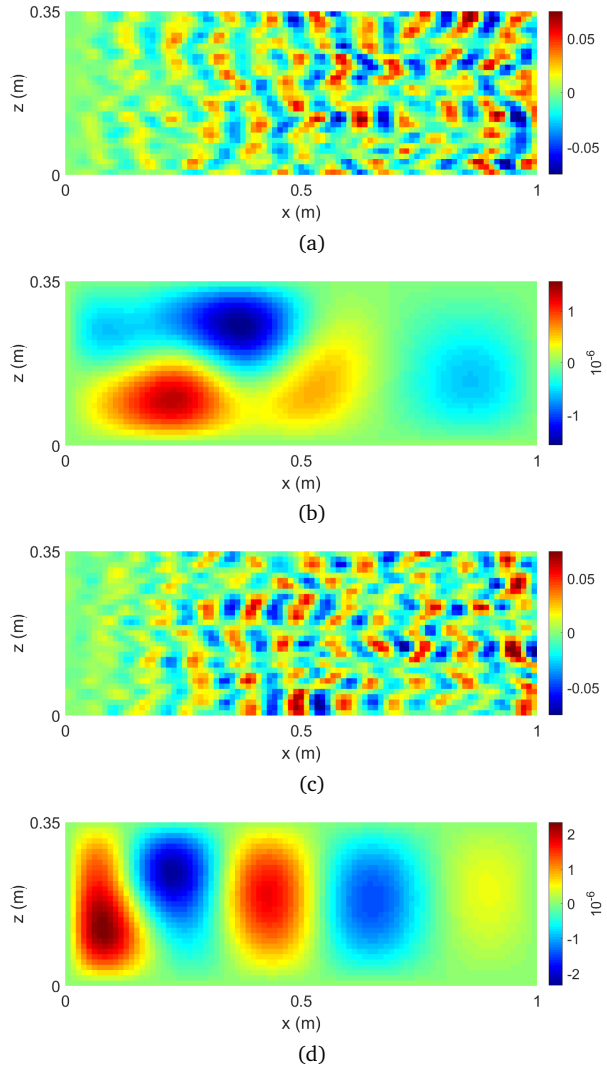

Figure 15: (a), (c): pressure fields (Pa) at the nodes of the spatial grid, generated by the C-UWPW method and (b), (d): their respective corresponding velocity fields (m/s), for an anti-resonance (277 Hz).

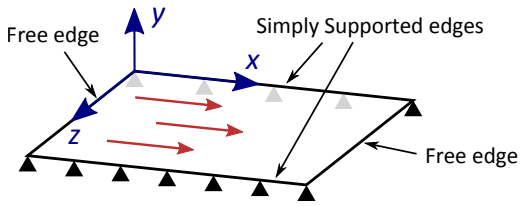

Figure 16: Rectangular panel with F-SS-F-SS boundary conditions.

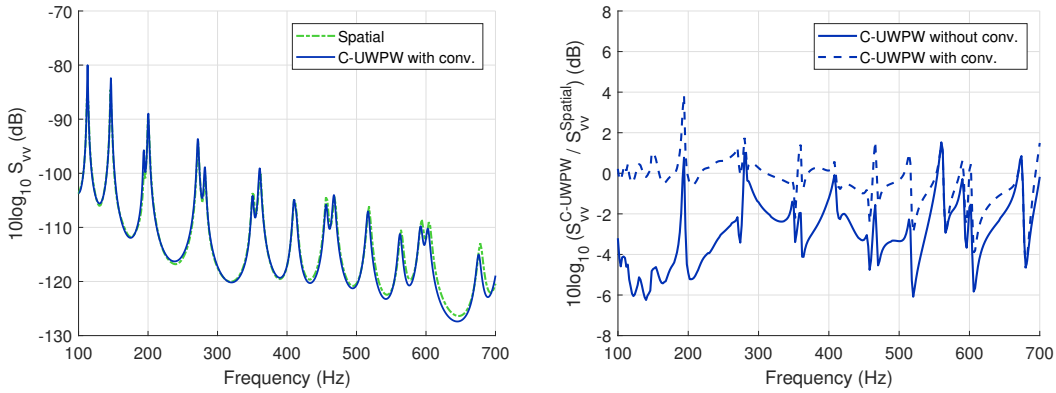

Figure 17: (a): Level of the spatial mean square velocity (dB, ref. $1\,(\mathrm{m/s})^2/\mathrm{Hz}$) calculated with the spatial method and the C-UWPW method including the convective contributions (30 realizations). Plate with F-SS-F-SS boundary condition. (b): Difference between the spatial method and the C-UWPW method with or without the convective contributions.

dimensions and the material remain unchanged, but the two edges of the panel perpendicular to the flow stream are set free, as represented in Fig. 16. The edges boundary conditions are free-simply supported-free-simply supported (F-SS-F-SS). As explained by Hambric et al. (2004), panels with free edges reacts more to the convective contributions of the WPF than the panels with simply-supported or clamped boundary conditions. In other words, the panel filtering effect in the wavenumber space is less significant for the former than for the latter.

The plate mean square velocity predicted with C-UWPW model is compared to the spatial one on Fig. 17. Compared to the simply supported plate considered in the previous sections, the resonant frequencies are shift toward the low frequencies. For instance, the third mode is moved from 159 Hz to 113 Hz. Fig. 17 shows a good agreement between the spatial results and the C-UWPW results when the convective contributions are taken into account. The small differences that can be observed in the higher part of the frequency range can be attributed to the finesse of the mesh used for the UWPW calculations that can not fully describe the small wavelength related to the convection. Fig. 17(b) shows that, if the convective contributions are neglected, the errors of the C-UWPW approach can be significant. In this case, the C-UWPW approach generally underestimates the plate velocity.

4.6. Influence of the non-homogeneity of the TBL

Finally, a last set of simulations is carried out for highlighting the effects of the non-homogeneity of the TBL on the panel vibratory response. The plate considered and the flow conditions is the one described in section 4.3 (i.e. plate with simply supported boundary conditions and a flow speed of 40 m/s). Results of calculations taking the spatial variations of the TBL into account are compared to the ones obtained by supposing that the TBL is homogeneous. The former results are obtained with the spatial and the C-UWPW approaches described in the section 3 whereas the latter ones are obtained with the spatial approach described in the section 2. The parameters for the supposed homogeneous TBL correspond to a spatial arithmetic mean of the varying TBL parameters: δ = 10.7 mm and τ = 3.76 Pa.

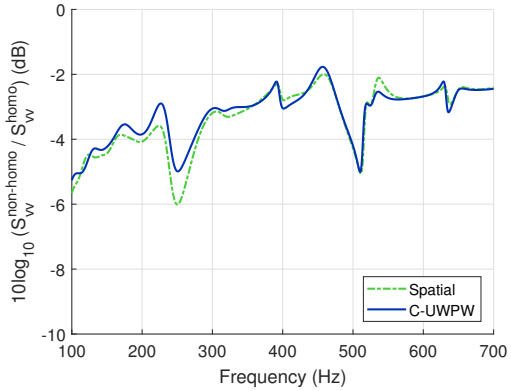

Figure 18: Difference of mean square velocity between non-homogeneous and homogeneous TBL for spatial and C-UWPW (30 realizations) approaches.

The differences of plate mean square velocity for the non-homogeneous TBL and for the supposed homogeneous TBL are plotted in Fig. 18. Three observations can be made: first, the curve related to the spatial approach and the one related to the C-UWPW approach are very close on the whole frequency range. This shows that the C-UWPW approach is well adapted to describe the effect of the spatial variations of the TBL on the plate vibrations. Second, significant differences (between 2 and 6 dB) can be observed on the whole frequency ranges between homogeneous and non-homogeneous cases. This shows that supposing the TBL as homogeneous can lead to important errors. Finally, the differences are not monotonic in frequency. For some particular frequencies (around 250 Hz and 510 Hz), the absolute differences can be significantly higher than for the others frequencies. They correspond to particular modes exhibiting deformations on the thinner part of the plate (i.e. close to the leading edge). As the TBL is growing from the leading edge, this thinner part is less excited than the rest of the panel and then these modes reacts less than in the case of a homogeneous TBL. This phenomena had already be observed with the SDT (see the reference Guillon et al. (2021) for more details on this aspect).

In terms of computing time, the spatial method has required 32 minutes per frequency point whereas only 1 minute has been necessary for the C-UWPW method. The former requires to calculate all the FRF between the couples of nodes of the FE mesh and to perform the double summation in Eq. (1) which are time consuming. In contrary, the C-UWPW method only requires to generate few realizations (typically 30) of the wall pressure field using Eq. (28), to calculate the vibroacoustic response of the panel to these pressure fields and to average the different responses. The reduction of the computing time of a factor greater by 50 is one of the main advantages of the C-UWPW method compared to the spatial one. Moreover, the C-UWPW is a non intrusive method. This means that it can be easily used with any vibroacoustic code. In the present case, the pressure fields have been calculated with MATLAB and have then be exported to be used as loadings of the MSC NASTRAN calculations. A last advantage of the method is that the same set of pressure fields can be used for different panels as long as the size of the panels and the flow conditions remain the same.

5. Conclusions

A numerical process has been proposed for predicting the response of vibrating structures excited by a non-homogeneous turbulent boundary layer. This original process make it possible to take into account the spatial variations of the TBL parameters in vibroacoustic simulations. It consists in a first step to generate different realizations of the random pressure fluctuations induced by the inhomogeneous TBL by using the analytical expression of Eq. (28). This expression gives the blocked pressure at a given node $\mathbf{X}$ of the vibroacoustic model from the spectrum of the WPF estimated with the TBL parameters at $\mathbf{X}$. In a second step, the different synthetized wall pressure fields of the inhomogeneous TBL are used as different loadings of the vibroacoustic model. Finally, after calculation of the vibroacoustic responses to the different loadings, an ensemble average of the different responses is performed to deduce the vibroacoustic response to the inhomogeneous TBL. This approach has been called the Continuously varying Uncorrelated Wall Plane Waves (C-UWPW) method as it consists in an extension of the UWPW technique developed some years ago for homogeneous TBL (Maxit, 2016).

The results of the C-UWPW method has been confronted to the ones obtained by the spatial approach and the Sub-area Decomposition Technique (SDT). This latter approach has been proposed recently by the present authors (Guillon et al., 2021) as a primary approach to take the non-homogeneous TBL into account and it has been used in the present paper as a base to develop the theoretical fundamentals of the C-UWPW method. The test case considered consisted in a rectangular plate excited on one side by a growing fully turbulent boundary layer triggered at one edge of the plate. The plate thickness was linearly varying in the stream-wise direction to stress the effect of the spatial evolution of the TBL. The following conclusions can be drawn from these comparisons:

- the C-UWPW results in term of plate vibratory response converges toward the ones of the spatial method as soon as 30 realizations are considered in the process;

- contrary to the SDT, the C-UWPW method can describe the convective contributions of the WPF when these ones have a significant influence of the panel response. However, as for the SDT, when these contributions can be neglected (for instance for frequencies well above the aerodynamic coincidence frequency for some panels), they can be easily filtered thanks to an appropriate cutoff wavenumber. This generally makes it possible to save significant computing time because a coarser mesh can be used in this case;

- the C-UWPW method is significantly less time consuming in term of computation that the spatial approach because it does not necessary to achieve a double summation on transfer functions that should be estimated between many nodes (see Eq. (3)). In the C-UWPW method, the number of vibroacoustic calculations is limited to the number of realizations considered. When the convective contributions can be neglected, the gain in computing times is even more important (due to use of a coarse mesh as evoked previously);

- comparison of a C-UWPW calculation describing the non-homogeneous TBL and another one supposing the TBL as homogeneous shows a significant difference (up to 6 dB) on the panel velocity response. This stresses the importance to take the spatial variations of the TBL parameters into vibroacoustic simulations, for instance with the proposed C-UWPW approach.

The investigations discussed in this paper will deserve to be continued in two directions in the future: first, the proposed approach has been validated by comparison with others numerical methods which are more time consuming. The gain in terms of computing is very significant. However, only an experimental validation would validate the whole process. In particular, the

vibration results depend on the accuracy of the WPF model considered in the calculation. At the authors' knowledge, experimental data allowing this validation are not available in the open literature. A dedicated study has to be carried out. The present approach could be used as a starting point to define plate cases highlighting the influence of the spatial variations of the TBL parameters (as the plate varying thickness considered in this paper). Wall pressure field, flow and vibration measurements will then be necessary on these cases in an aerodynamic or hydrodynamic tunnel; second, a case without static pressure gradient has been considered as it allowed us using the zero pressure gradient models of the WPF deeply studied and validated in the literature. However, the cases of non-homogeneous TBL resulting of pressure gradients are commonly met in practice. The proposed approach could be applied to these cases as soon as accurate models of the WPF in adverse or favorable pressure gradients will be available. The developments of these WPF models are then in the natural prolongation of the present work.

Acknowledgment

This work was supported by the French ministry of armed forces, under the responsibility of the Agence de l'Innovation et de la Défense, and performed within the framework of the Labex CeLyA of Université de Lyon, supervised by the French National Research Agency (ANR-10-LABX-0060/ ANR-11-IDEX-0007).

References

Bonness, W.K., Capone, D.E., Hambric, S.A., 2010. Low-wavenumber turbulent boundary layer wall-pressure measurements from vibration data on a cylinder in pipe flow. Journal of Sound and Vibration 329, 4166–4180.

Bull, M.K., 1996. Wall-pressure fluctuations beneath turbulent boundary layers: some reflections on forty years of research. Journal of Sound and Vibration 190, 299–315.

Chase, D., 1980. Modeling the wavevector-frequency spectrum of turbulent boundary layer wall pressure. Journal of Sound and Vibration 70, 29–67.

Ciappi, E., De Rosa, S., Franco, F., Vitiello, P., Miozzi, M., 2016. On the dynamic behavior of composite panels under turbulent boundary layer excitations. Journal of Sound and Vibration 364, 77–109.

Ciappi, E., Magionesi, F., 2005. Characteristics of the turbulent boundary layer pressure spectra for high-speed vessels. Journal of Fluid and Structures 21, 321–333.

Ciappi, E., Magionesi, F., De Rosa, S., Franco, F., 2009. Hydrodynamic and hydroelastic analyses of a plate excited by the turbulent boundary layer. Journal of Fluid and Structures 25, 321–342.

Ciappi, E., Magionesi, F., De Rosa, S., Franco, F., 2012. Analysis of the scaling laws for the turbulence driven panel responses. Journal of Fluid and Structures 32, 90–103.

Cohen, E., Gloerfelt, X., 2018. Influence of pressure gradients on wall pressure beneath a turbulent boundary layer. Journal of Fluid Mechanics 838, 715–758.

Corcos, G., 1964. The structure of the turbulent pressure field in boundary-layer flows. Journal of Fluid Mechanics 18, 353–378.

De Rosa, S., Franco, F., 2008. Exact and numerical responses of a plate under a turbulent boundary layer excitation. Journal of Fluid and Structures 24, 212–230.

De Rosa, S., Franco, F., Ciappi, E., 2013. PEDE^{M}: a new method for the analysis of the stochastic response. Aerotecnica Missili & Spazio 92, 87–93.

De Rosa, S., Franco, F., Ciappi, E., 2015. A simplified method for the analysis of the stochastic response in discrete coordinates. Journal of Sound and Vibration 339, 359–375.

Franco, F., De Rosa, S., Ciappi, E., 2013. Numerical approximations of the predictive responses of plates under stochastic and convective loads. Journal of Fluid and Structures 42, 296–312.

Goody, M., 2004. Empirical spectra model of surface pressure fluctuations. American Institute of Aeronautics and Astronautics Journal 42, 1788–1794.

Graham, W., 1997. A comparison of models for the wavenumber-frequency spectrum of turbulent boundary layer pressures. Journal of Sound and Vibration 206, 541–565.

Guillon, C., Maxit, L., Redon, E., 2021. Modeling vibrating panels excited by a non-homogeneous turbulent boundary layer. Journal of Fluid and Structures 116, 103378.

Hambric, S.A., Hwang, Y., Bonness, W.K., 2004. Vibrations of plates with clamped and free edges excited by low-speed turbulent boundary layer flow. Journal of Fluid and Structures 19, 93–110.

Hong, C., Shin, K.K., 2010. Modeling of wall pressure fluctuations for finite element structural analysis. Journal of Sound and Vibration 329, 1673–1685.

Hwang, Y., Bonness, W.K., Stephen Hambric, S.A., 2009. Comparison of semi-empirical models for turbulent boundary layer wall pressure spectra. Journal of Sound and Vibration 319, 199–217.

Karimi, M., Croaker, P., Maxit, L., Robin, O., Skvortsov, A., Marburg, S., Kessissoglou, N., 2020a. A hybrid numerical approach to predict the vibrational responses of panels excited by a turbulent boundary layer. Journal of Fluid and Structures 92, 102814.

Karimi, M., Maxit, L., Meyer, V., Marburg, S., Kirby, R., 2020b. Non-negative intensity for planar structures under stochastic excitation. Journal of Sound and Vibration 488, 115652.

Lin, J., Zhang, Y., Zhao, Y., 2011. Pseudo Excitation Method and some recent developments. Procedia Engineering 14, 2453–2458.

Marchetto, C., Maxit, L., Robin, O., Berry, A., 2018. Experimental prediction of the vibration response of panels under a turbulent boundary layer excitation from sensitivity functions. Journal of the Acoustical Society of America 143, 2954–2964.

Maury, C., Gardonoio, P., Elliott, S., 2002. A wavenumber approach to modelling the response of a randomly excited panel, part I: general theory. Journal of Sound and Vibration 252, 83–113.

Maxit, L., 2016. Simulation of the pressure field beneath a turbulent boundary layer using realizations of uncorrelated plane waves. Journal of the Acoustical Society of America 140, 1268–1285.

Maxit, L., Berton, M., Audoly, C., Juvé, D., 2015. Discussion about different methods for introducing the turbulent boundary layer excitation in vibroacoustics models, in: Flinovia - Flow Induced Noise and Vibration Issues and Aspects, Springer. pp. 249–278.

Maxit, L., Denis, V., 2013. Prediction of flow induced sound and vibration of periodically stiffened plates. Journal of the Acoustical Society of America 133, 146–160.

Mellen, R.H., 1990. On modeling convective turbulence. Journal of the Acoustical Society of America 88, 2891–2893.

Rozenberg, Y., Robert, G., Moreau, S., 2012. Wall-pressure spectral model including the adverse pressure gradient effects. American Institute of Aeronautics and Astronautics Journal 50, 2168–2179.

Salze, E., Bailly, C., Marsden, O., Jondeau, E., Juvé, D., 2014. An experimental characterization of wall pressure wavevector-frequency spectra in the presence of pressure gradients, in: 20th AIAA/CEAS Aeroacoustics Conference, p. 2909.

Sanders, M., 2014. The Boundary Layer over a Flat Plate. Bachelor thesis. University of Twente. Netherland.

Schilchting, H., Gersten, K., 2017. Boundary-Layer Theory. 9 ed., Springer.

Strawderman, W.A., 1969. Turbulence-induced plate vibrations: an evaluation of finite- and infinite-plate models. Journal of the Acoustical Society of America 46, 1294–1307.

Xu, Y., Zhang, W., Ko, J., Lin, J., 1999. Pseudo-excitation method for vibration analysis of wind-excited structures. Journal of Wind Engineering and Industrial Aerodynamics 83, 443–454.